# ASIC Waveform Receiver with Improved Environmental Tolerance for Probing Space Plasma Waves in Environments with High Radiation and Wide Temperature Variation

***Yuya Tokunaga[1], Mitsunori Ozaki[1], Satoshi Yagitani[1], Hiroki Koji[1], Daisuke Yonetoku[1], Takahiro Zushi[2], and Hirotsugu Kojima[3]***

[1]Kanazawa University, Ishikawa, Japan
Kakuma-machi, Kanazawa 920-1192, Japan
E-mail:ozaki@is.t.kanazawa-u.ac.jp

[2]Department of Electrical Engineering
National Institute of Technology, Nara College

[3]Research Institute for Sustainable Humanosphere
Kyoto University

## Abstract

Plasma-wave observations are conducted under conditions of high radiation and wide temperature variation. The electrical characteristics of plasma-wave instruments should therefore be insensitive to these environmental factors. We have developed a new application-specific integrated circuit (ASIC) waveform receiver with a rad-hard [radiation-hardened] amplifier and a temperature-compensation circuit. The environmental tolerance of the conventional ASIC receiver is unsuitable for probing plasma waves in the range 1 Hz to 10 kHz in harsh space environments. Its weak radiation tolerance under 350 krad results in radiation-induced degradation in noise performance, such that weak plasma waves are lost in the noise floor. With an ambient temperature change of −40° C to +100° C, the gain response of the conventional ASIC receiver varies by more than ±1.0 dB, preventing accurate measurement of plasma waves around the cutoff frequency of 10 kHz. Our new ASIC receiver operates at a total dose rate of 350 krad without degradation in noise performance. Moreover, the temperature dependence of the gain response from −60° C to +100° C dramatically improved by ±0.05 dB due to the addition of a compensation circuit. Our new ASIC receiver can contribute to the measurement of plasma waves in challenging environmental conditions to further the understanding of magnetospheric dynamics.

## 1. Introduction

The Earth's radiation belts consist of relativistic particles trapped by geomagnetic fields [1]. Bombardment by high-energy relativistic particles affects the electrical systems within satellites (e.g., GPS) [2]. Plasma-wave observations are important for understanding the relationship between plasma waves and radiation-belt formation. Multipoint plasma-wave observations have been conducted using multi-satellites (e.g., Cluster [3], THEMIS [4], and MMS [5]). However, the spatial resolution of multi-satellite observations is too low for plasma-wave probing due to the insufficient number of satellites for the plasma wavelength. Poor spatial resolution could be improved by launching more satellites at lower cost. Application-specific integrated circuit (ASIC) technology has been applied to plasma-wave observations (e.g., dc [6] and ac [7-9] magnetic-field observations), providing dramatic reductions in mass, volume, and power.

This study deals with a plasma waveform receiver [10-12] connected to electromagnetic sensors (e.g., search-coil magnetometers [13] and wire-probe antennas [14]), and high-sensitivity preamplifiers. Fukuhara et al. [11] previously described an ASIC-based plasma waveform receiver. However, the output dynamic range, radiation tolerance, and temperature dependence of conventional

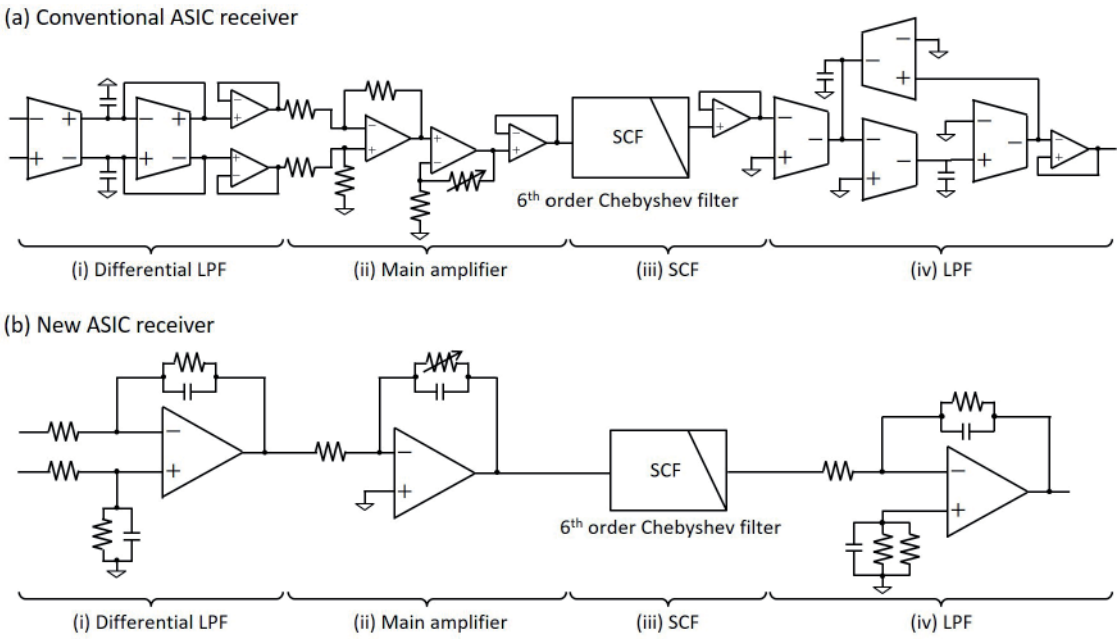


**Figure 1. The schematic block diagrams of the conventional (a) and new (b) ASIC receivers.**

ASIC receivers are inadequate for plasma-wave observations. These require a flat gain response from 1 Hz to 10 kHz with sharp cutoff characteristics and a wide dynamic range of 2.6 Vpp (approximately 80% of the 3.3 V supply voltage). The gain response of a conventional ASIC receiver is not flat, having a large ripple of 2.0 dB generated by the sharp cutoff of a sixth-order Chebyshev filter. The narrow output dynamic range of a conventional ASIC receiver is 45% of its 3.3 V supply voltage. The gain response of the conventional ASIC receiver can be smoothed by redesigning the transfer function, but without buffering to expand its dynamic range, the amplifier cannot output waveforms of amplitude greater than 45% of the 3.3 V supply voltage. Hence, the conventional ASIC receiver cannot deliver the required electrical performance. Furthermore, the ASIC receiver must be able to operate within harsh space environments to accurately capture plasma waves.

Ozaki et al. [9] developed an ASIC preamplifier for plasma-wave observations that could tolerate the extreme environments of space. Our target for environmental tolerance is almost identical to that of Ozaki et al. [9], to use the new ASIC receiver connected to a search-coil magnetometer via the ASIC preamplifier for probing plasma waves. We performed a radiation test for an experimental ASIC receiver. The SS520-3 sounding rocket used the experimental ASIC receiver. The SS520-3 sounding rocket will launch to detect in situ wave-particle interactions causing the ion outflow phenomena at the cusp. The observation targets are electric fields in the VLF range below 10 kHz. In this study, the receiver was used to estimate the radiation tolerance of a conventional ASIC receiver, which is discussed in Section 4. The noise performance of the experimental receiver was degraded following radiation tests with 350 krad total dose rate. From the radiation test results, the radiation tolerance of the conventional ASIC receiver was found to be inadequate. Testing the conventional ASIC receiver across the temperature range −40° C to +100° C, we confirmed it to have a large temperature-dependent gain response of over ±1.0 dB.

To improve the electrical performance and environmental tolerance of the conventional ASIC receiver, in this study we redesigned its transfer function and replaced the conventional amplifier with a new operational amplifier (OPA). We designed the new operational amplifier to be approximately twice the size of the conventional amplifier to improve its radiation tolerance, and we added a temperature-compensation circuit [9] to minimize temperature dependence.

Our new ASIC receiver achieved a flat gain response with a ripple of 0.8 dB or less, and a wide dynamic range of 2.7 Vpp: 82% of the 3.3 V supply voltage. The receiver demonstrated a radiation tolerance of 350 krad or more, and a gain response with an ultra-low temperature dependence of 0.05 dB or less.

## 2. ASIC Receiver

The schematic circuit diagrams of the conventional and new ASIC receivers are shown in Figure 1. In each design, stage (i) is a differential low-pass filter (LPF) to remove common-mode noise and to limit the bandwidth. Stage (ii) is a main amplifier to adjust the system gain. Stage (iii) is a sixth-order Chebyshev low-pass switched-capacitor filter (SCF) to prevent aliasing. The cutoff frequency of the switched-capacitor filter can be controlled by its clock frequency. In this study, we applied a 1 MHz clock signal

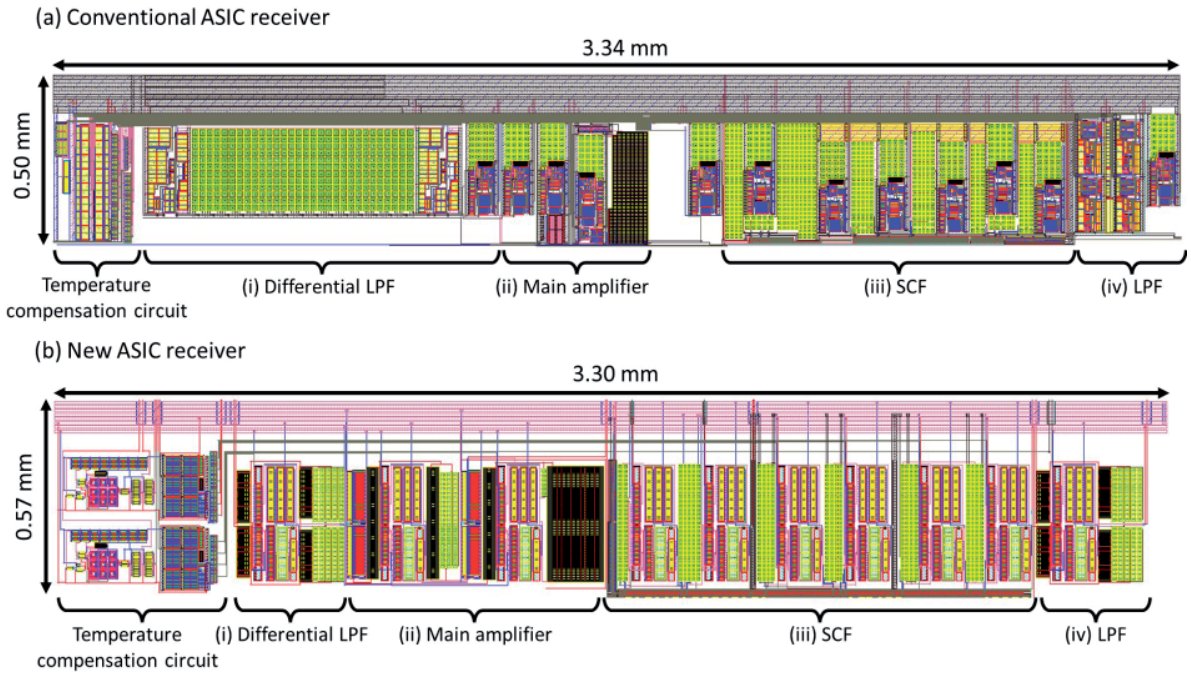


**Figure 2. The layouts of the conventional (a) and new (b) ASIC receivers.**

of 3.3 Vpp to the switched-capacitor filter to tune the cutoff frequency to 10 kHz. The final stage (iv) is a low-pass filter to reduce ringing from the switched-capacitor filter clock. Stages (i) and (iv) of the conventional ASIC receiver are Gm-C low-pass filters, based on operational transconductance amplifiers (OTAs). We replaced the Gm-C filters with active low-pass filters based on the new operational amplifier to improve the ASIC receiver's dynamic range. The existing operational transconductance amplifier, without output buffering, had a narrow dynamic range. Our new amplifier was two times larger than the conventional amplifier to reduce its radiation absorbed dose, which is discussed in Section 4.

As plasma waves propagate in three-dimensional space, plasma-wave measurements demand a three-axis electromagnetic sensor. The size of a three-channel ASIC receiver is limited to a bare die size of 5 mm × 5 mm. Figure 2 shows the layouts of the conventional and new ASIC receivers. Both green areas of stages (i) in Figure 2 show the metal-insulator-metal capacitors. The capacitor area of new stage (i) was smaller than the conventional are because of changing the cutoff frequencies from 170 kHz to 300 kHz. The size of the new ASIC receiver was 0.57 mm × 3.30 mm, which was close to that of the conventional ASIC receiver and within the acceptable range. Power consumption figures for the conventional and new ASIC receivers were 20 mW and 25 mW, respectively. The 5 mW increase was due to the addition of the new amplifiers and a temperature-compensation circuit. The conventional ASIC receiver had a temperature-compensation circuit different from that of the new receiver. However, the conventional switched-capacitor filter was supplied not by the compensation circuit but by an external resistance, which was not sufficient for supplying reference currents corresponding to ambient temperature.

## 3. Electrical Characteristics of ASIC Receiver

The ASIC receiver required a flat gain response between 1 Hz and 10 kHz, with a sharp cutoff at 10 kHz, and a low pass-band ripple of 1.0 dB or less, to capture plasma waves without aliasing. Figure 3 shows the gain response of the conventional and new ASIC receivers. Both simulations in Figure 3 were performed with a *Tanner EDA* circuit simulator [15]. In the gain simulations, we calculated both gains using the harmonic ratio between output and input waveforms when inputting a 100 Hz clock waveform. For each receiver, the gain response of the switched-capacitor filter clock was simulated using transient rather than ac analysis. Both sets of results were plotted from 100 Hz to 100 kHz to reduce the memory required for the circuit simulations. The conventional ASIC receiver exhibited significant pass-band ripple of 2.0 dB. The measurements in Figure 3a displayed a 2.5 dB difference between calculated and simulated values due to the output impedance of the conventional amplifier [11]. The large ripple could cause the conventional ASIC receiver's output to saturate. The new ASIC receiver displayed flat gain characteristics up to the cutoff frequency of 10 kHz, with a low ripple of 0.8 dB, as shown in Figure 3b.

Figure 4 shows the input-output characteristics of the conventional and new ASIC receivers. The conventional ASIC receiver had a narrow output dynamic range of 1.5 Vpp, which was 45% of the 3.3 V supply voltage.

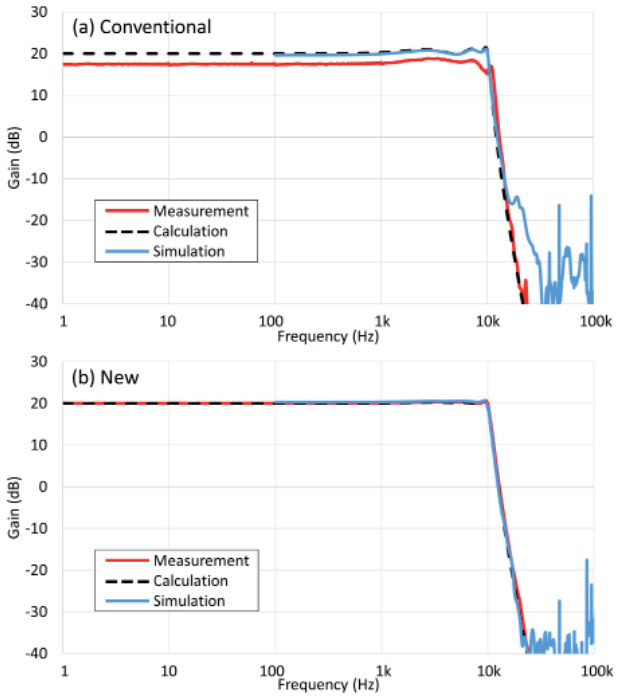


**Figure 3. The measured (red solid lines), calculated (black dashed lines), and simulated (blue solid lines) gain-response results for the conventional (top) and new (bottom) ASIC receivers.**

To improve this, we designed the new ASIC receiver to use operational amplifiers, increasing the dynamic range by 80% to 2.7 Vpp. Figure 5 shows the measured output waveforms for the conventional and new ASIC receivers for a 1 kHz 0.25 Vpp sine-wave input. The narrow dynamic range of the conventional ASIC receiver caused the output to saturate, but the new ASIC receiver sufficiently amplified the sine waves. The output voltage of the ideal operational transconductance amplifier and operational amplifier are given by [16]

$$V_{inp} - V_{ov1} < V_{OTA} < V_{power} - V_{ov2}, \quad (1)$$

$$V_{ov3} < V_{OPA} < V_{power} - V_{ov4}, \quad (2)$$

where $V_{inp}$ is the positive input voltage of the operational transconductance amplifier; $V_{ov1}$, $V_{ov2}$, $V_{ov3}$, and $V_{ov4}$ are the CMOS overdrive voltages; $V_{OTA}$ is the output voltage; $V_{power}$ is the ASIC receiver power supply voltage; and $V_{OPA}$ is the operational amplifier output voltage. In both ASIC receivers, $V_{inp}$, $V_{ov1}$, $V_{ov2}$, $V_{ov3}$, $V_{ov4}$, and $V_{power}$ are approximately 1.65 V, 0.1 V, 0.2 V, 0.2 V, 0.4 V, and 3.3 V, respectively. The input voltage, $V_{inp}$, was set at the common voltage of the conventional ASIC receiver to consist of the fourth stage (iv) based on the single-ended operational transconductance amplifier from Figure 1a. The voltages $V_{OTA}$ and $V_{OPA}$ in Equations (1) and (2) ranged from 1.55 V to 3.1 V and from 0.2 V to 2.9 V, respectively. An ideal output dynamic range for the operational transconductance amplifier was 1.55 Vpp, which was 4.82 dB lower than that of the operational amplifier. Moreover, as shown in Figure 1a, the operational transconductance amplifier needed a voltage follower due to its high output impedance of 300 kΩ, which could otherwise couple to stray capacitance and pick up noise. From Equation (2), the ideal output dynamic range of the new ASIC receiver was 2.7 Vpp, which was the same as the measurement shown in Figure 4. The low output impedance of the operational amplifier was 10 kΩ for driving the large output buffer current of 320 μA. We measured total harmonic distortion (THD) by inputting 5 kHz sine waves of 0.12 Vpp and 0.09 Vpp into the ASIC receivers, under which input conditions both receivers could output a 1.0 Vpp sine wave. Both ASIC receivers displayed total harmonic distortion degradation at 5 kHz due to the presence of ripple at 10 kHz, which was the second harmonic of a

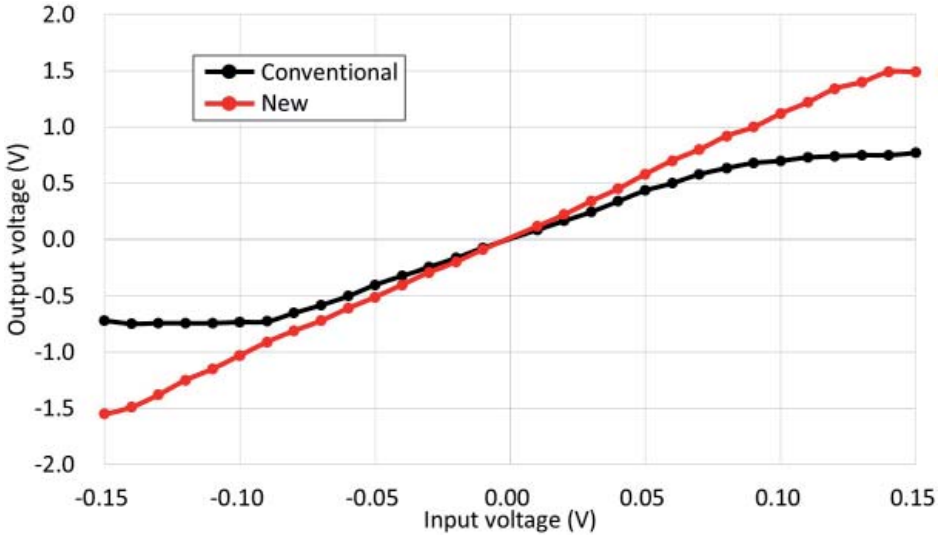


**Figure 4. The input-output characteristics of the conventional (black line) and new (red line) ASIC receivers.**

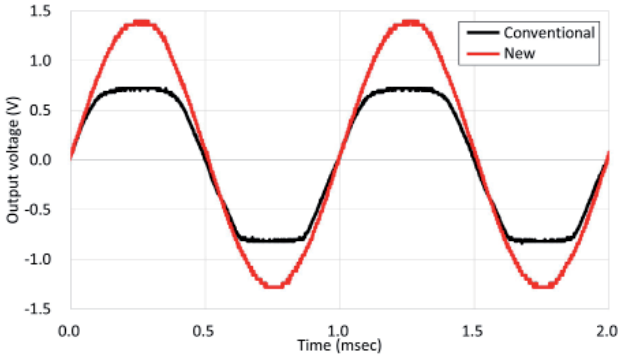


**Figure 5. The output waveforms at 1 kHz for the conventional (black line) and new (red line) ASIC receivers.**

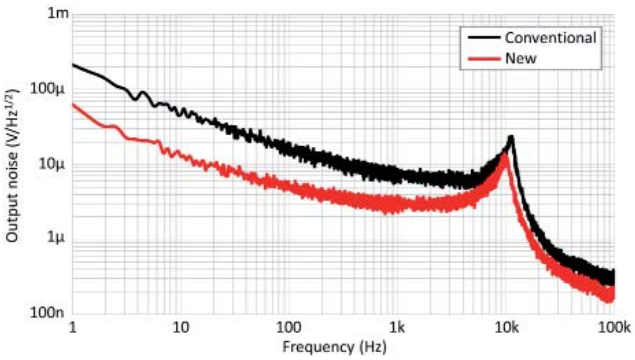


**Figure 6. The output noise of the conventional (black line) and new (red line) ASIC receivers.**

distorted 5 kHz sine wave. The total harmonic distortion of the conventional and new ASIC receivers was 20 dB and 42 dB, respectively. The measured slew rates of the conventional and new ASIC receivers were 0.01 V/µsec and 0.03 V/µsec, respectively.

As shown in Figure 1a, the conventional ASIC receiver includes several capacitors between signal and ground lines. We assumed charging and discharging of these to be responsible for the slow slew rate. When outputting a 1.0 Vpp sine wave, both receivers put out waveforms below 3.18 kHz and 9.55 kHz without the slew-rate limitation. The new ASIC receiver displayed reduced total harmonic distortion at 5 kHz due to the suppression of ripple between 2.0 dB and 0.8 dB and an improved slew rate. Figure 6 shows the output noise of both receivers. We evaluated their noise performance using output noise rather than equivalent input noise due to the switched-capacitor filters being the dominant noise source. Low output noise is preferable for probing weak plasma waves. The new receiver offered improved output-noise performance between 1 Hz and 10 kHz. In particular, its output noise at 1 Hz was 10 dB lower than that of the conventional ASIC receiver. The voltage noise spectral density of CMOS is described as per [17]

$$e_n = \sqrt{\frac{k_f}{2C_{ox}WLf}\frac{1}{f} + \frac{8}{3}kT\frac{1}{g_m}}, \quad (3)$$

where $k_f$ is the flicker noise coefficient, $C_{ox}$ is the gate capacitance per unit area, $W$ and $L$ are the gate width and length, $f$ is the frequency, $k$ is the Boltzmann constant, $T$ is the absolute temperature, and $g_m$ is the CMOS transconductance. The first and second terms in Equation (3) dominate in the frequency range of flicker noise from 1 Hz to 1 kHz and thermal noise over 1 kHz, respectively. Flicker noise is reduced by increasing the gate dimensions, $WL$ $WL$ ; the resulting amplifier design had a larger surface area and lower output noise than the original.

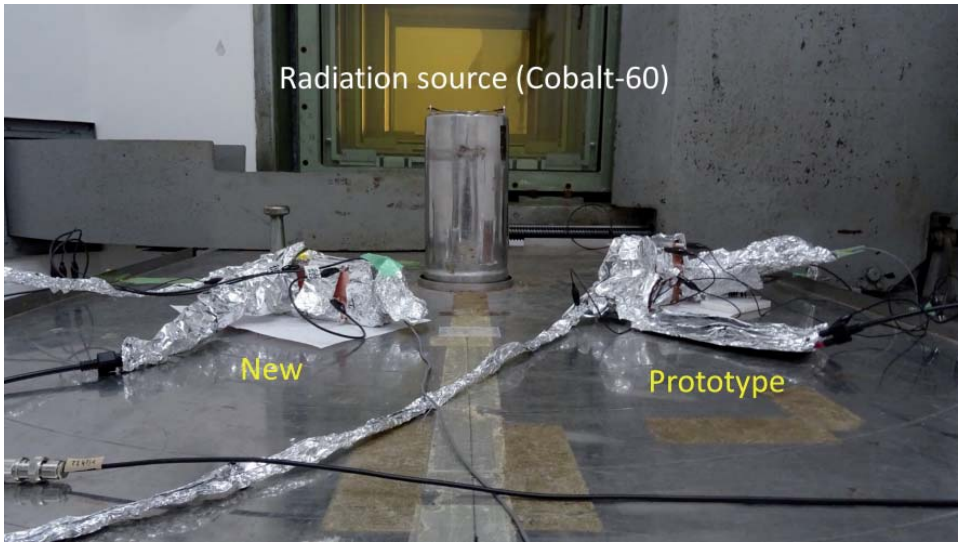


**Figure 7. The radiation test setups for the conventional and new ASIC receivers.**

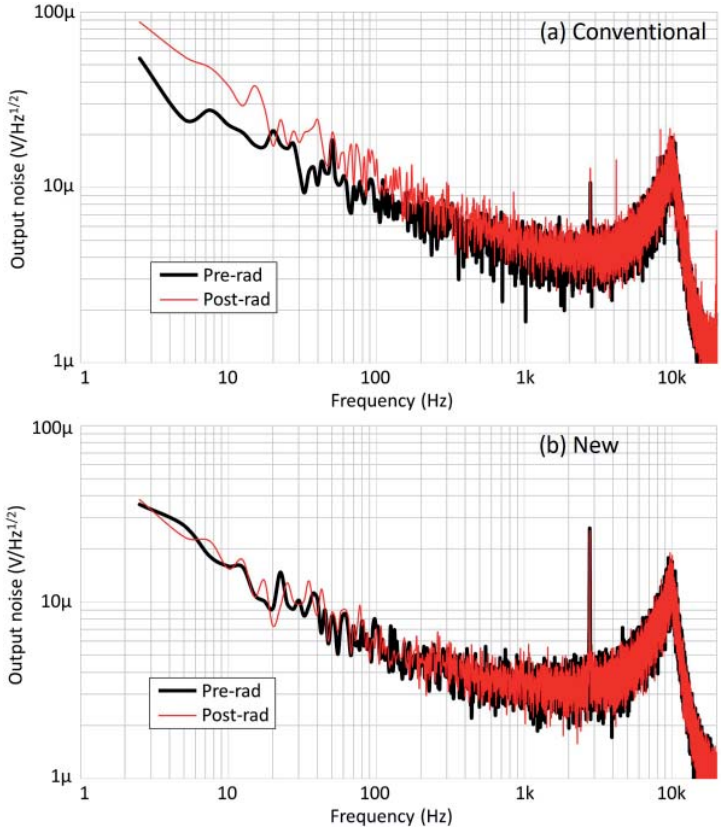


**Figure 8. The radiation test results for the conventional (a) and new (b) ASIC receivers.**

## 4. Radiation Tolerance

In space environments, plasma-wave instruments are exposed to high-energy particles of several hundred MeV [18]. The effects of radiation on the ASIC receiver degrade its noise characteristics. To design a rad-hard amplifier for the new ASIC receiver, we evaluated the relationship between amplifier surface area and radiation absorbed dose using a particle and heavy ion transport code system (*PHITS*) radiation simulator [19]. Radiation affects amplifiers by entering their gate oxide films ($SiO_2$) [20]. In the radiation simulation models, we used $SiO_2$ plates to model the two amplifier designs. Both simulation models had the same surface area as the CMOS area of the two amplifiers. The first model was 0.5 mm × 0.5 mm, and the second was 0.7 mm × 0.7 mm. The thickness of both models was assumed to be 10 nm. A pencil beam was used as a gamma radiation source.

From the simulation results, the total dose rate for the model with 0.7 mm × 0.7 mm surface area was approximately 0.5 times lower than that of the model with 0.5 mm × 0.5 mm surface area. The surface area ratio of 0.5 mm × 0.5 mm to 0.7 mm × 0.7 mm is approximately 0.5, which was the same ratio as the total dose rate between both simulation models. The total dose rate depends on the surface area of the $SiO_2$ plate: Increasing the $SiO_2$ surface area decreases the amplifier's total dose rate. The amplifier in the new ASIC receiver was designed to be approximately twice as large as that of the conventional ASIC receiver to provide improved radiation tolerance.

To evaluate the conventional receiver's radiation tolerance, the experimental ASIC receiver was exposed to gamma ray from cobalt-60 at the Radioisotope Research Center, Tokyo Institute of Technology. Figure 7 shows the radiation test setup for the new ASIC receiver and the experimental receiver. The switched-capacitor filter of the experimental ASIC receiver was similar to that of the conventional ASIC receiver. The noise of the switched-capacitor filter was dominant in both ASIC receivers.

Figure 8 shows the pre- and post-radiation output noise levels for the experimental receiver and new ASIC receivers. Both ASIC receivers were exposed to total dose rates of up to 350 krad. As shown in Figure 8a, the experimental receiver's output noise was degraded between 2.5 Hz and 1 kHz following the radiation tests. Output noise degradation was 4.0 dB at 2.5 Hz. The radiation test results can be described by the CMOS voltage noise density Equation (3). The degradation in output noise below 1 kHz in the conventional ASIC receiver was possibly due to the gate capacitance per unit area, $C_{ox}$, in Equation (3) having decreased by 0.4 times its pre-rad value as a result of charged particles from the gamma ray becoming trapped in the gate-oxide films. Conversely, we theorized that the output noise of the new ASIC receiver

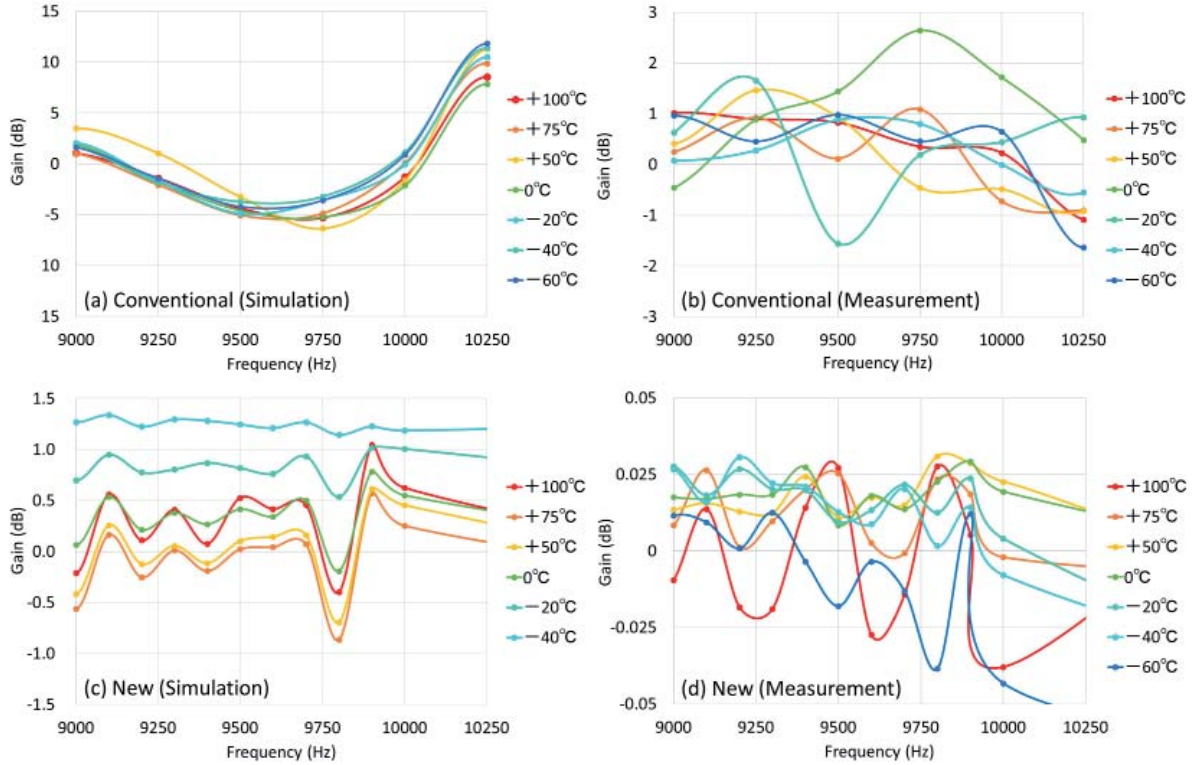


**Figure 9. The simulated (a, c) and measured (b, d) temperature-dependence results for the conventional (top) and new (bottom) ASIC receivers.**

was unchanged by the radiation tests due to the increased recombination rate of the larger amplifier. Gamma rays cause the transconductance, $g_m$, in Equation (3) of both ASIC receivers to decrease, generating interface states. A decrease in $g_m$ leads to degraded output noise performance. However, in both receivers, output noise over 1 kHz was not affected by gamma rays. We selected a process (TSMC 0.25 μm CMOS) with a thinner gate-oxide film for both ASIC receivers to prevent generation of interface states. As shown in Figure 8, the conventional ASIC receiver was unable to tolerate radiation of 350 krad and over, while the new ASIC receiver showed no degradation of output noise performance following the radiation test. The new amplifier design with a CMOS surface area twice as large as that of the conventional amplifier effectively decreased the radiation absorbed dose and improved the radiation tolerance of the conventional ASIC receiver.

## 5. Stability in Thermal Variation

The gain response of the ASIC receiver was affected by ambient temperature variation, making measured plasma-wave amplitudes ambiguous. A constant gain with no temperature dependence was hence required. To evaluate the temperature dependence of both ASIC receivers, a *Tanner EDA* circuit simulator [15] was used. Figure 9 shows the temperature dependence relative to a +25° C reference point for the gain responses of both ASIC receivers. It should be noted that the range of the vertical axis for both receivers is different in Figure 9. The fluctuation for the new receiver was much smaller. As shown in the simulation results in Figure 9a, the conventional ASIC's temperature dependence was high due to the 2.0 dB pass-band ripple and the CMOS threshold voltage variation based on ambient temperature.

As shown in Figure 3, redesigning the switched-capacitor filter transfer function reduced the ripple from 2.0 dB to 0.8 dB. When the pass-band ripple in Figure 3 was shifted by a change in ambient temperature, the temperature dependence of the conventional ASIC receiver was greater than that of the new ASIC receiver. Reference currents should correspond to a threshold voltage variation of approximately ±10% from +25° C to −60° C and to +100° C. A bias resistance of 32 kΩ provided the reference currents of the conventional ASIC receiver.

We performed temperature simulations from −60° C to +100° C to evaluate the temperature-induced variation in the reference currents supplied by the bias-resistance and temperature-compensation circuit. From those simulations, the calculated rate of variation of the reference current from standard temperature at +25° C was approximately ±6% across the temperature range. We designed a temperature-compensation circuit without external bias resistance to supply reference currents depending on ambient temperatures [9]. The rate of variation of the reference current from the temperature-compensation circuit increased by approximately ±30% across the temperature range. Reference-current variation of ±30% across the range −60° C to +100° C corresponded with a 10% variation in threshold voltage due to ambient temperature.


**Figure 10a. The temperature test setup for the conventional ASIC receiver.**

Comparing the simulation results in Figures 9a and 9c, the temperature dependence of the new ASIC receiver with the temperature-compensation circuit improved significantly from ±15.0 dB to ±3.0 dB.

Figure 10 shows the temperature test setup for the conventional and new ASIC receivers. The temperature tests for the conventional and new ASIC receivers were conducted in ETAC FL420N (Kusumoto Chemicals, Ltd.) thermostatic chambers at Kanazawa University and MC-712 (ESPEC Corp.) at the National Institute of Technology, Ishikawa College, respectively. As per the temperature test results in Figures 9b and 9d, the temperature dependence of the new ASIC receiver drastically decreased to ±0.05 dB compared to the conventional ASIC receiver due to suppression of the pass-band ripple and compensation for temperature-induced variation in CMOS threshold voltage. These temperature test results indicated that the compensation circuit effectively reduced temperature dependence, minimizing the impact of wide temperature variations in space environments on the gain response of the new ASIC receiver.

## 6. Conclusion

We developed a rad-hard amplifier and a temperature-compensation circuit to improve the environmental tolerance of a conventional ASIC receiver. By replacing Gm-C filters with active low-pass filters, the new ASIC receiver's dynamic range expanded significantly from 1.5 Vpp to 2.7 Vpp, which was over 80% of the 3.3 V supply voltage. Because of this wide dynamic range and flat gain response from 1 Hz to 10 kHz with low pass-band ripple, the new ASIC receiver probes plasma waves without saturation. Based on the environmental test results, our new ASIC receiver demonstrated radiation tolerance of 350 krad or more and ultra-low temperature dependence


**Figure 10b. The temperature test setup for the new ASIC receiver.**

of ±0.05 dB variation in gain response in the range −60° C to +100° C.

The vibration and vacuum tests assuming the SS520-3 sounding rocket experiment were conducted to evaluate the robustness of the experimental ASIC receiver. The difference between the experimental receiver and the new ASIC receiver was the amplifiers comprising the switched-capacitor filter. During both the tests, the experimental receiver operated efficiently without any breakdowns. We consider the new ASIC receiver and the experimental receiver to be equally robust. Plasma waves have nonlinear temporal characteristics that are the key to understanding magnetospheric dynamics. Plasma-wave amplitude and phase information detected by the Arase (ERG) satellite [21, 22] contributed to the observation of the relationship between chorus waves and the auroral phenomena [23, 24]. The waveform receiver connected to the search-coil magnetometer of the Arase satellite covered the frequency range from 1 Hz to 20 kHz [22]. The new ASIC receiver operates over the same frequency range as the waveform receiver by inputting a 2 MHz clock. With its wide dynamic range and high environmental tolerance, our new ASIC receiver is therefore eminently suitable for obtaining accurate plasma-wave observations in high radiation environments and across wide temperature variations. The new ASIC receiver will contribute toward understanding the formation of radiation belts in harsh space environments.

## 7. Acknowledgments

This study was supported by Grant-in-Aid for Scientific Research (15H02136, 17H06140, and 17K06456) from the Japan Society for the Promotion of Science; by a research grant for Exploratory Research on Sustainable Humanosphere Science from Research Institute for Sustainable Humanosphere, Kyoto University; and a research grant from Sakigake project, Kanazawa University. This study was also supported by VLSI Design and Education Center, the University of Tokyo, with the collaboration of Cadence Design Systems, Inc., and Mentor Graphics Corporation. This study was also supported by Japan Atomic Energy Agency for the radiation simulation

by the *PHITS* code. The authors also thank Mr. I. Yoda of Radioisotope Research Center, Tokyo Institute of Technology, for his support and cooperation during the radiation tests. The authors also thank Prof. T. Fukami and Dr. R. Higashi of National Institute of Technology Ishikawa College, for their help during the temperature tests.

## 8. References

1. Y. Y. Shprits, R. B. Horne, A. C. Kellerman and A. Y. Drozdov, "The Dynamics of Van Allen Belts Revisited," *Nature Physics*, **14**, 1, February, 2018.

2. R. B. Horne, S. A. Glauert, N. P. Meredith, D. Boscher, V. Maget, D. Heynderickx, and D. Pitchford, "Space Weather Impacts on Satellites and Forecasting the Earth's Electron Radiation Belts with SPACECAST," *Space Weather*, **11**, January 2013, pp. 169-186.

3. G. Gustafsson, R. Boström, B. Holback, G. Holmgren, A. Lundgren, K. Stasiewicz, L. Åhlén, F. S. Mozer, D. Pankow, P. Harvey, P. Berg, R. Ulrich, A. Pedersen, R. Schmidt, A. Butler, A. W. C. Fransen, D. Klinge, M. Thomsen, C.-G. Fälthammar, P.-A. Lindqvist, S. Christenson, J. Holtet, B. Lybekk, T. A. Sten, P. Tanskanen, K. Lappalainen, and J. Wygant, "The Electric Field and Wave Experiment for the Cluster Mission," *Space Science Reviews*, **79**, January 1997, pp. 137-156.

4. V. Angelopoulos, "The THEMIS Mission," *Space Science Reviews*, December 2008.

5. R. B. Torbert, C. T. Russell, W. Magnes, R. E. Ergun, P.-A. Lindqvist, O. LeContel, H. Vaith, J. Macri, S. Myers, D. Rau, J. Needell, B. King, M. Granoff, M. Chutter, I. Dors, G. Olsson, Y. V. Khotyaintsev, A. Eriksson, C. A. Kletzing, S. Bounds, B. Anderson, W. Baumjohann, M. Steller, K. Bromund, Guan Le, R. Nakamura, R. J. Strangeway, H. K. Leinweber, S. Tucker, J. Westfall, D. Fischer, F. Plaschke, J. Porter, and K. Lappalainen, "The FIELDS Instrument Suite on MMS: Scientific Objectives, Measurements, and Data Products," *Space Science Reviews*, **199**, March 2016, pp. 105-135.

6. W. Magnes, M. Oberst, A. Valavanoglou, H. Hauer, C. Hagen, I. Jernej, H. Neubauer, W. Baumjohann, D. Pierce, J. Means, and P. Falkner, "Highly Integrated Front-End Electronics for Spaceborne Flux Gate Sensors," *Measurement Science and Technology*, **19**, September 2008.

7. A. Rhouni, G. Sou, P. Leroy, and C. Coillot, "Very Low 1/f Noise and Radiation Hardened CMOS Preamplifier for High-Sensitivity Search Coil Magnetometers," *IEEE Sensors Journal*, **13**, January, 2013, pp. 159-166.

8. M. Ozaki, S. Yagitani, H. Kojima, K. Takahashi, and A. Kitagawa, "Current-Sensitive CMOS Preamplifier for Investigating Space Plasma Waves by Magnetic Search Coils," *IEEE Sensors Journal*, **14**, February, 2014, pp. 421-429.

9. M. Ozaki, S. Yagitani, H. Kojima, K. Takahashi, H. Kouji, T. Zushi and Y. Tokunaga, "Development of an ASIC Preamplifier for Electromagnetic Sensor Probes for Monitoring Space Electromagnetic Environments," *Earth, Planets and Space*, **28**, May, 2016, pp. 68-91.

10. H. Kojima, H. Fukuhara, Y. Mizuochi, S. Yagitani, H. Ikeda, Y. Miyake, H. Usui, H. Iwai, Y. Takizawa, Y. Ueda, H. Yamakawa, "Miniaturization of Plasma Wave Receivers Onboard Scientific Satellites and Its Application to the Sensor Network System for Monitoring the Electromagnetic Environments in Space," *Advances in Geosciences*, **21**, 2010, pp. 461-481.

11. H. Fukuhara, H. Kojima, H. Ishii, S. Okada, and H. Yamakawa, "Tiny Waveform Receiver with a Dedicated System Chip for Observing Plasma Waves in Space," *Measurement Science and Technology*, **23**, September 2012.

12. T. Zushi, H. Kojima, K. Onishi, M. Ozaki, S. Yagitani, S. Shimizu, and H. Yamakawa, "Small Sensor Probe for Measuring Plasma Waves in Space," *Earth, Planets and Space*, **67**, August 2015, pp. 67-127.

13. O. Le Contel, P. Leroy, A. Roux, C. Coillot, D. Alison, A. Bouabdellah, L. Mirioni, L. Meslier, A. Galic, M. C. Vassal, R. B. Torbert, J. Needell, D. Rau, I. Dors, R. E. Ergun, J. Westfall, D. Summers, J. Wallace, W. Magnes, A. Valavanoglou, G. Olsson, M. Chutter, J. Macri, S. Myers, S. Turco, J. Nolin, D. Bodet, K. Rowe, M. Tanguy, B. de la Porte, "The Search-Coil Magnetometer for MMS," *Space Science Reviews*, **199**, March, 2016, pp. 257-282.

14. Y. Kasaba, K. Ishisaka, Y. Kasahara, T. Imachi, S. Yagitani, H. Kojima, S. Matsuda, M. Shoji, S. Kurita, T. Hori, A. Shinbori, M. Teramoto, Y. Miyoshi, T. Nakagawa, N. Takahashi, Y. Nishimura, A. Matsuoka, A. Kumamoto, F. Tsuchiya and R. Nomura, "Wire Probe Antenna (WPT) and Electric Field Detector (EFD) of Plasma Wave Experiment (PWE) Aboard the Arase Satellite: Specifications and Initial Evaluation Results," *Earth, Planets and Space*, **69**, December, 2017.

15. TannerEDA, "Mentor Graphics Japan Co., Ltd.," https://www.mentorg.co.jp/tannereda/, accessed on January 7, 2020.

16. R. Jacob Baker, *CMOS: Circuit Design, Layout, and Simulation (Third Edition)*, New York, IEEE Press, 2010.

17. P. E. Allen and D. R. Holberg, *CMOS Analog Circuit Design, Second Edition*, New York, Oxford Univ. Press, 2002.

18. R. M. Millan and D. N. Baker, "Acceleration of Particles to High Energies in Earth's Radiation Belts," *Space Science Reviews*, **173**, November 2012, pp. 103-131.

19. T. Sato, Y. Iwamoto, S. Hashimoto, T. Ogawa, T. Furuta, S. Abe, T. Kai, P. Tsai, N. Matsuda, H. Iwase, N. Shigyo, L. Sihver and K. Niita, "Features of Particle and Heavy Ion Transport code System (PHITS) Version 3.02," *J. Nucl. Sci. Technol*, **55**, 5, January, 2017, pp. 684-690.

20. T. R. Oldham and F. B. McLean, "Total Ionizing Dose Effects in MOS Oxides and Devices," *IEEE Trans. Nucl. Sci.*, **50**, 9, July, 2003.

21. M. Ozaki, S. Yagitani, Y. Kasahara, H. Kojima, Y. Kasaba, A. Kumamoto, F. Tsuchiya, S. Matsuda, A. Matsuoka, T Sasaki and T. Yumoto," Magnetic Search Coil (MSC) of Plasma Wave Experiment (PWE) Aboard the Arase (ERG) Satellite," *Earth, Planets and Space*, **70**, 4, May, 2018.

22. Y. Kasahara, Y. Kasaba, H. Kojima, S. Yagitani, K. Ishisaka, A. Kumamoto, F. Tsuchiya, M. Ozaki, S. Matsuda, T. Imachi, Y. Miyoshi, M. Hikishima, Y. Katoh, M. Ota, M. Shoji, A. Matsuoka and I. Shinohara, "The Plasma Wave Experiment (PWE) on Board the Arase (ERG) satellite," *Earth, Planets and Space*, **70**, 21, May, 2018.

23. M. Ozaki, K. Shiokawa, Y. Miyoshi, K. Hosokawa, S. Oyama, S. Yagitani, Y. Kasahara, Y. Kasaba, S. Matsuda, R. Kataoka, Y. Ebihara, Y. Ogawa, Y. Otsuka, S. Kurita, R. C. Moore, Y. M. Tanaka, M. Nosé, T. Nagatsuma, M. Connors, N. Nishitani, Y. Katoh, M. Hikishima, A. Kumamoto, F. Tsuchiya, A. Kadokura, T. Nishiyama, T. Inoue, K. Imamura, A. Matsuoka, I. Shinohara, "Microscopic Observations of Pulsating Aurora Associated with Chorus Element Structures: Coordinated Arase Satellite-PWING Observations," *Geophysical Research Letters*, **45**, 12, November, 2018. pp. 12,125-12,134.

24. M. Ozaki, Y. Miyoshi, K. Shiokawa, K. Hosokawa, S. Oyama, R. Kataoka, Y. Ebihara, Y. Ogawa, Y. Kasahara, S. Yagitani, Y. Kasaba, A. Kumamoto, F. Tsuchiya, S. Matsuda, Y. Katoh, M. Hikishima, S. Kurita, Y. Otsuka, R. C. Moore, Y. Tanaka, M. Nosé, T. Nagatsuma, N. Nishitani, A. Kadokura, M. Connors, T. Inoue, A. Matsuoka and I. Shinohara, "Visualization of Rapid Electron Precipitation via Chorus Element Wave–Particle Interactions," *Nature Communications*, **10**, 16, January, 2019.